Corrigendum to "Facile one-pot synthesis of platinum nanoparticles decorated nitrogen-doped graphene with high electrocatalytic performance for oxygen reduction and anodic fuels ox…

ARTICLE *in* JOURNAL OF POWER SOURCES · FEBRUARY 2015

Impact Factor: 6.22 · DOI: 10.1016/j.jpowsour.2014.11.117

Journal of Power Sources 277 (2015) 268–276

Contents lists available at ScienceDirect

Journal of Power Sources

journal homepage: www.elsevier.com/locate/jpowsour

Facile one-pot synthesis of platinum nanoparticles decorated nitrogen-graphene with high electrocatalytic performance for oxygen reduction and anodic fuels oxidation

Aso Navaee [a], Abdollah Salimi [a, b, *], Saeid Soltanian [b, c], Peyman Servati [c]

[a] Department of Chemistry, University of Kurdistan, 66177-15175 Sanandaj, Iran
[b] Research Center for Nanotechnology, University of Kurdistan, 66177-15175 Sanandaj, Iran
[c] Department of Electrical and Computer Engineering, University of British Columbia, 2332 Main Mall, Vancouver, BC V6T 1Z4, Canada

HIGHLIGHTS

- A one-step synthesis of N-doped graphene decorated with Pt-nanoparticles was reported.
- The GCE/N-Gr/PtNP exhibits excellent electrocatalytic activity toward O_2 reduction.
- GCE/N-Gr/PtNP shows high electrocatalytic activity to alcohols, N_2H_4, HCOOH oxidation.
- N-Gr/PtNP lower poisoning/deactivation compared to commercial 10% carbon-Pt catalyst.
- This method can be developed to preparation of N-Gr decorated with other novel metals.

GRAPHICAL ABSTRACT

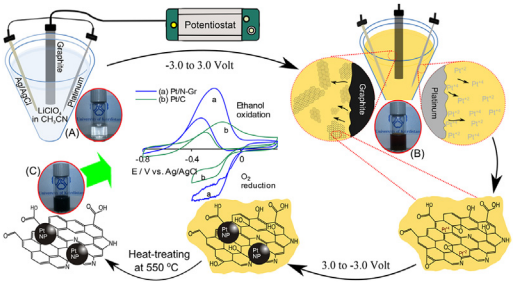

ARTICLE INFO

Article history:
Received 30 July 2014
Received in revised form
19 November 2014
Accepted 25 November 2014
Available online 26 November 2014

Keywords:
Nitrogen doped-Graphene
Platinum nanoparticles
Electrocatalysis
Oxygen reduction
Anodic fuels oxidation

ABSTRACT

Due to exceptional electronic properties of graphene (Gr) and nitrogen doped graphene (N-Gr), they are considered as superior supporting platforms for novel metal nanoparticle decorations. Here, we report, a novel one-step electrochemical method for synthesis of Nitrogen-doped graphene sheets uniformly decorated with platinum nanoparticles (Pt/N-Gr). A graphite rod and platinum wire are respectively used for graphene and platinum nanoparticles production. The potential is cycled from −3V to +3V in acetonitrile solution as a nitrogen dopant source. By increasing the number of cycles the nitrogen-doped graphene/platinum nanoparticles composite is generated. After heat-treating the composite is characterized with various techniques such as FTIR, Raman, XPS, SEM and TEM. The electrocatalytic activity of the prepared composite toward the reduction of O_2 and the oxidation of usual anodic fuels such as methanol, ethanol, hydrazine and formic acid is investigated using cyclic voltammetry technique. In comparison to commercial platinum/carbon, the onset potentials and the current densities for both O_2 reduction and fuels oxidation are remarkably improved. Furthermore, the modified electrode by this composite shows good long-term stability and poisoning tolerance.

* Corresponding author. Department of Chemistry, University of Kurdistan, 66177-15175 Sanandaj, Iran. Tel.: +98 8733634001; fax: +98 8733634001.
E-mail address: absalimi@uok.ac.ir (A. Salimi).

http://dx.doi.org/10.1016/j.jpowsour.2014.11.117
0378-7753/

1. Introduction

The electrochemical oxygen reduction reaction (ORR) is an important process in fuel cells, metal-air batteries, water purification, oxygen detection and corrosion protection [1–3]. On the other hand, ethanol and methanol, as sources of energy greener than fossil-fuels, have been directly used as fuel without external reformer in direct alcohol fuel cells [4]. In addition, direct formic acid and hydrazine fuel cells have also been attractive for portable device applications due to their several advantages such as high theoretical open circuit voltage (about 1.61 V for N_2H_4–O_2 and 1.45 V for CH_2O_2–O_2), low fuel crossover, low toxicity and high energy efficiency (~80%) [5–7]. Therefore, hydrazine and formic acid have been considered as fuels for alkaline and acidic fuel cells, respectively. Ammonia (NH_3) is another fuel with theoretical cell potential of 1.17 V at 25 °C [8], which compared to N_2H_4–O_2 or HCOOH–O_2, is slightly lower. Furthermore, the normal boiling point of ammonia is −33.34 °C whereas; the boiling point of hydrazine is 114 °C. Therefore, in comparison to ammonia, hydrazine is a nonvolatile compound and may be more efficient fuel for room temperature alkaline fuel cell. However, the development of durable electrocatalysts with high activity and cost-effective for ORR and fuel oxidation reaction (FOR) is a challenge. In this regard, tremendous efforts have been made to develop simple, compatible and suitable catalysts with high activity and fast kinetic reaction rate for fuel cell applications. Carbon supported platinum catalyst (Pt/C) is the main commercially available catalyst as cathode and anode materials for ORR and FOR, respectively. However, Pt/C suffers from many limitations such as slow oxidation kinetics of FOR and deactivation due to the formation of CO or other unidentified intermediate during the fuels oxidation [9,10]. On the other hand, the agglomeration or detachment of platinum catalyst from support materials decreases the fuel cell performance. Therefore, in recent years, different strategies have been proposed for the improvement of catalytic activities and also, development of the novel synthetic techniques for the production of new bimetallic or metal free electrocatalysts with less susceptibility to poisoning intermediates [7,11–13]. Furthermore, different metal oxides such as CeO_2, RuO_2, SnO_2 or antimony doped thin oxide (Sb_2O_5 SnO_2, ATO) on carbon black has been used for the supporting of Pt as anode catalysts for direct alcohol fuel cells [14,15].

The physical, chemical and structural properties of supports play important roles not only in distribution and stabilization of the catalyst particles but also in diffusion kinetics of reactants and products in a catalytic system [16]. Recently various kinds of carbon materials including carbon black, carbon nanotubes, graphitized carbon materials and Gr have been used as catalyst support for fuel cells [17]. Among carbon-based materials, Gr appears to be an excellent electrocatalyst candidate for fuel cells due to superior electrical conductivity, excellent mechanical flexibility, chemical stability, remarkable thermal conductivity, high surface-to-volume ratio and monolayer thickness [18–21]. Furthermore, some of the mentioned properties of Gr can be improved via chemical functionalization of surface or edge defects [22]. For the modulation of electronic properties and as a consequence, improving the electrocatalytic behavior of Gr, recent studies have focused either on doping with heteroatoms such as nitrogen, boron, sulfur, selenium and phosphorus [23–25]. Among the various dopant atoms, boron and nitrogen, which have comparable atomic size with carbon atom, can form strong covalence bond with carbon atoms. Also, it has been demonstrated that nitrogen is the better dopant rather than boron for the enhancement of electronic and optical properties of Gr [26] due to the π-delocalization. In addition, the experimental evidences and quantum mechanical calculations indicated that substitution of nitrogen atoms in the carbon frameworks of electrodes, especially in the form of pyridinic and graphitic quaternary nitrogen, significantly enhance their electrocatalytic activity for ORR [13,27–29], as well as their resistance to CO and methanol poisoning. It is expected that nitrogen-doped graphene (N-Gr) can be useful for the supporting of metal catalyst such as Pt, where N-Gr supported Pt nanoparticles have been used as effective electrocatalyst for fuel cells [30–32] and sensing applications [34].

Numerous complicated methods such as chemical vapor deposition (CVD), arc-discharge, thermal and hydrothermal annealing of graphene oxide (GO) under an ammonia atmosphere have been developed to produce N-Gr sheets [23–25,27–35]. On the other hand, several methods have been reported for preparation of Gr and N-Gr decorated with Pt nanoparticles and their application for the fuel cells design [17,30–32,36–38]. The above mentioned techniques involve several complex steps, require high vacuum and commonly produce a mixture of multilayer and single layer N-Gr sheets. These methods are usually costly, convoluted and involve several steps such as Gr synthesis, N doping process, Pt synthesis and decorating process. However, implementing efficient methods to synthesis heteroatom-doped-Gr fallowed by decorating with metal nanoparticles have been a challenge. Thus, development the novel facile methods for synthesis of N-Gr or N-Gr decorated with Pt nanoparticles is highly desirable and also, commercially and technologically important.

Here, we demonstrate, for the first time, a novel and direct one-pot electrosynthesis of N-Gr decorated with Pt nanoparticles (Pt/N-Gr). Cyclic voltammetry technique is used in a conventional electrochemical cell with graphite rod and platinum wire as electrodes and acetonitrile as a solvent and nitrogen source. The prepared composite material is systematically characterized with various microscopic and spectroscopic instruments. The electrocatalytic ability and durability of prepared composite toward ORR and oxidation of methanol, ethanol, formic acid and hydrazine is examined and compared with commercial Pt/C (10% Pt).

2. Experimental

2.1. Materials and electrochemical instrument

The graphite rod, graphite powder, acetonitrile, lithium perchlorate, phosphate buffer salts, sulfuric acid solution, potassium hydroxide and commercial platinum on activated carbon with 10% of Pt loading (Pt/C 10%) were purchased from Merck. The electrolyte solution including 0.1 M KOH, 0.1 M phosphate and 0.1 M H_2SO_4 were prepared from commercial resources which were obtained from Merck. The platinum wire, which was used as counter electrode and mass source for production of platinum nanoparticles, was purchased from Metrohm. The electrochemical synthesis of Pt/N-Gr and all electrochemical studies including cyclic voltammetry, linear sweep voltammetry with rotating electrode and amperometry were carried out using a μAUTOLAB modular electrochemical system (ECO Chemie, Ultrecht, The Netherlands) equipped with a PGSTAT 101 module driven by GPES software (ECO Chemie) in conjunction with a conventional three-electrode system (an Ag/AgCl/3 M KCl and platinum wire as reference and counter electrode, respectively) and a personal computer for data acquisition and processing. For modification of glassy carbon (GC) electrode with Pt/N-Gr and Pt/C, 5 μL of dispersed solution of these materials (5 mg ml^{-1} in ethanol) was cast on the electrode surface and dried at room temperature. To achieve nitrogen and oxygen saturated solution before each experiment, the electrolyte solution was purged by nitrogen or oxygen gas for 5 min. Scan rates for recorded cyclic voltammograms was 0.02 V s^{-1} and all experiments were done at room temperature (~298 K).

2.2. Structural characterization

UV–vis and fluorescence spectra of samples were obtained by an SPECTROD 250-analytikjena spectrophotometer (Germany) and an EL01044753-Varian spectrophotometer (USA), respectively. The FTIR spectra of KBr discs containing 0.1 mg of prepared nanomaterials before and after the heat-treating process as well as chemically synthesized Gr powders were obtained by a Vector-22 BRUKER spectrophotometer (Switzerland). Raman spectrometry was carried out by a SENTERRA system (Laser power of 25 mW, BRUKER, Germany). XPS measurements were performed with a Leybold MAX200 analyzer with vacuum in the range of 10^{-9} torr, using achromatic Al K-alpha X-ray. Curve fitting of the XPS spectra was performed using the Gaussian–Lorentzian peak fit software. Transmission electron microscopy (TEM) was performed with a FEI Tecnai microscope operated at 200 kV. Field emission-scanning electron microscopy (FE-SEM) images with operating voltage of 20.0 kV were obtained with a Zeiss Sigma.

2.3. Synthesis of Pt/N-Gr

GO was synthesized using modified hummers method as described in our previous work [39]. In brief, 1 g graphite powder was added to 3 g of $NaNO_3$ and 70 ml of concentrated H_2SO_4 and stirred for 30 min in an ice bath. Then, 3 g $KMnO_4$ was gradually added at 15 min under stirring. The mixture was stirred for 2 h at ambient temperature and then diluted with DI water and stirred for 30 min. After that, 5% H_2O_2 was added into the solution until the color of the mixture changed to yellow (in web version), indicating that graphite was fully oxidized. Afterward, the GO nanosheets were reduced by hydrazine. As schematically shown in Fig. 1, to produce the Pt/N-Gr nanohybride, potential cycling is performed over a potential window of ±3.0 V at scan rate of 0.3 V s^{-1} in the pure acetonitrile containing 0.5 M $LiClO_4$ as a supporting electrolyte. A graphite rod (with diameter of ~8 mm) and Pt wire (with diameter of ~2 mm) were used as working and counter electrodes, respectively and an Ag/AgCl/KCl 3 M was used as a reference electrode. The Pt wire was placed at a distance of 2 mm from graphite rod in electrochemical cell. With increasing the number of potential cycles (performed from −3 to +3 V), the thin Gr sheets were released from the surface of graphite rod and the solution gradually changed from colorless to yellowish brown (in web version) (Fig. 1A, B). Based on our understanding and previous reports [40], the ±3.0 V is high enough to oxidize the ClO_4^- ions and consequently, the CH_3CN molecules into the radical forms. During the potential scan to the positive direction, the ClO_4^- could be appeared as an electron transfer mediator and hence, oxidized to radical forms ($ClO_4^{\cdot}$). Then, the reaction of $ClO_4^{\cdot}$ with solvent produces acetonitrile radicals ($CH_2CN^{\cdot}$) based on the following equations:

$$ClO_4^- \rightarrow ClO_4^{\cdot} + e \quad (1)$$

$$ClO_4^{\cdot} + CH_3CN \rightarrow HClO_4 + {}^{\cdot}CH_2CN \quad (2)$$

The resulting radicals are able to oxidize the graphite rod and platinum wire. The oxidation is followed by intercalating of solvent and electrolyte components, leading to extricate Pt^{+n} and thin platelets of Gr. Consequently, on one hand, the free Pt^{+n} ions are rapidly complexed by acetonitrile molecules [41], and then surrounded by Gr sheets. On the other hand, the carbon atoms on the Gr edges are attacked by $CH_2CN^{\cdot}$ to form Gr-$CH_2CN^{\cdot}$. The potential cycling on the negative direction assists the formation of uniform *Pt* nanoparticles on the Gr sheets via reduction of $Pt^{+n}(CH_3CN)_m$ complex as well as formation of either pyridine or pyrrole rings on the edges or defective sites of the Gr monolayers.

After 1500 potential cycles the solution was centrifuged and washed with a mixture of double distilled water and ethanol for 5 times to remove solvent and electrolyte ions, and then, dried at 80–90 °C. The remaining dark-brown materials was heat-treated at 550 °C for 10 min in an electrical furnace, and then washed 3 times with a mixture of boiling deionized water and 0.1 M H_2SO_4. Thermal treatment of the as-prepared materials facilitates recovery of the π-network of N-Gr and evaporates any remaining acetonitrile, which trapped by Pt/N-Gr nanostructure, as well as removes non-cyclic nitrogen atoms located on the edges of Gr sheets. The efficiency of the method was achieved about 0.2 g of Pt/N-Gr per 1500 potential cycles. The final product (a black powder) was dispersed in ethanol for further examinations (Fig. 1C).

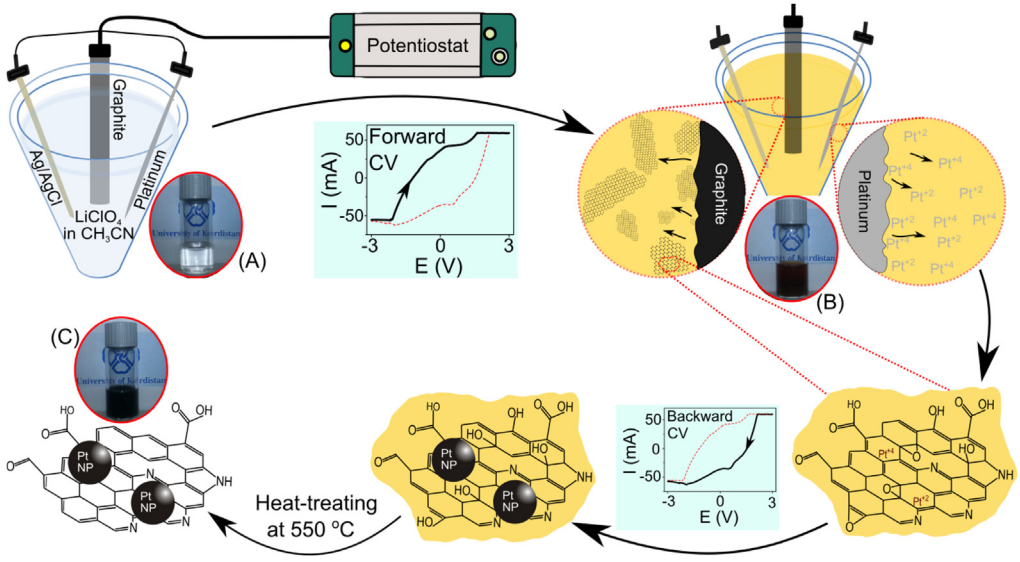

Fig. 1. Schematic of the electrochemical methods for Pt/N-Gr synthesis, illustrating (A) the initial colorless solution of pure acetonitrile containing 0.5 M $LiClO_4$, (B) the yellowish brown solution after 1500 cycle, and (C), the final Pt/N-Gr product dispersed in ethanol. (For interpretation of the references to color in this figure legend, the reader is referred to the web version of this article.)

3. Results and discussion

3.1. Characterization of materials

UV–vis absorption and luminescence spectrum (Figure S1) of the as-synthesized Pt/N-Gr and GO reveals that they have different chemical nature (see Supporting information). Also, recorded cyclic voltammetry (CV) of those samples over −0.3 to 0.5 V demonstrates significant differences in electrochemical properties of the as prepared and heat-treated materials (Figure S2). Fig. 2A compares the FTIR spectra of the as-prepared Pt/N-Gr before and after heat-treating process and chemically synthesized GO. The differences are more pronounced at 3455, 1660, 1482 and 1116 cm^{-1} that are attributed to N–H, C=N, N=O and C–N, respectively (see also Supporting information and Figure S3). As seen in the Raman spectra of the Pt/N-Gr and GO (Fig. 2B), a D band (at ~1340 cm^{-1}) and a G band (at ~1605 cm^{-1}) are observed which are associated to the sp^3 defect sites and sp^2-bonded pairs (C=N and C=C), respectively [3,23]. In comparison to GO (with I_D/I_G = 1.29), the Pt/N-Gr exhibits higher I_D/I_G (1.34) and also broader G band, implying the intercalation of N and Pt atoms into Gr. The two additional peaks at 695 and 549 cm^{-1} are also attributed to metal complexes [42] due to covalent bonds formation between platinum atoms and N-Gr structures.

X-ray photoelectron spectroscopy (XPS) spectra of Gr and Pt/N-Gr are shown in Fig. 2C. Apart from the carbon and oxygen bands, two distinct bands are observed at binding energy (BE) of about 75 and 400 eV attributed to platinum 4f and nitrogen 1s, respectively.

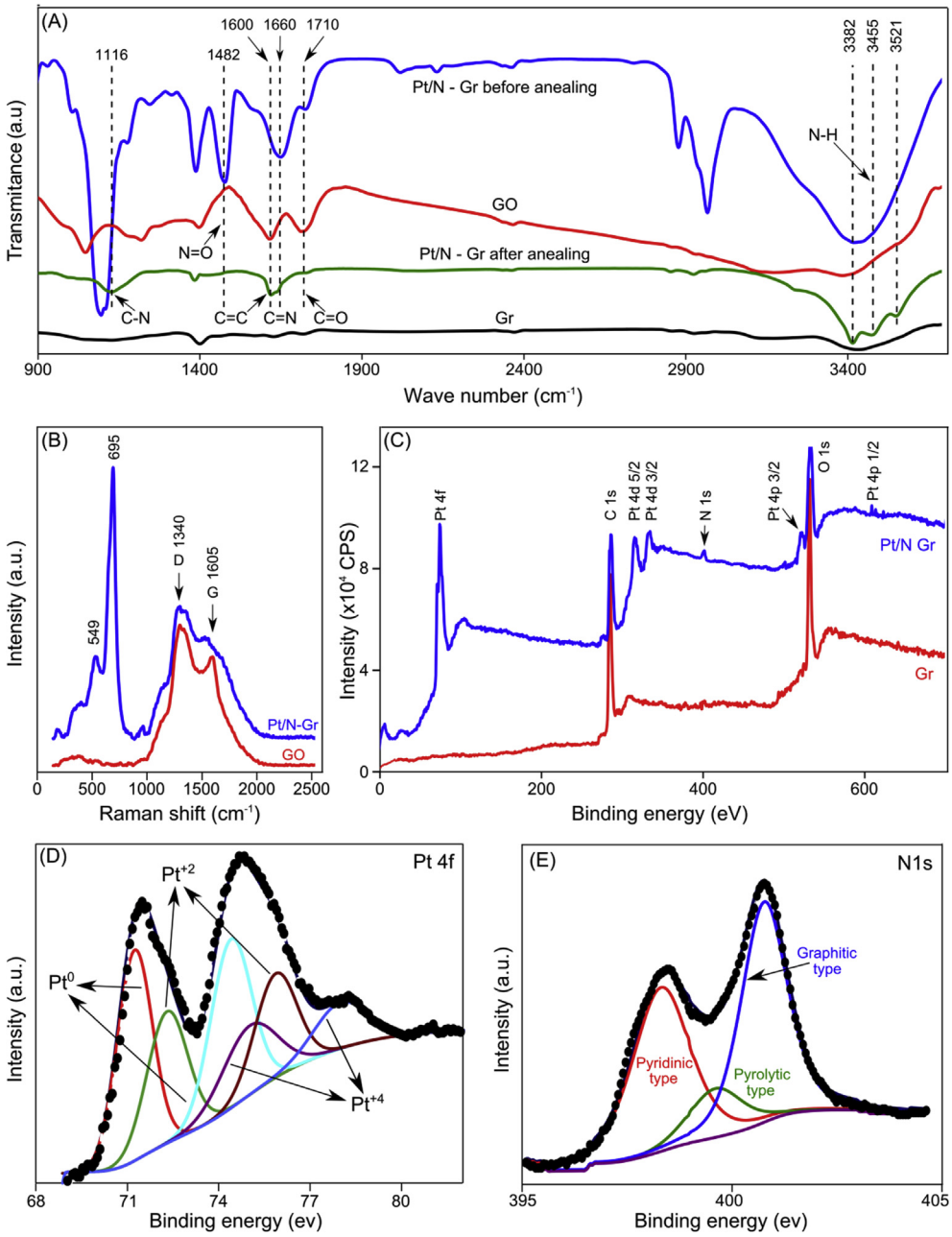

Fig. 2. A) FTIR spectra of Pt/N-Gr before and after the heat-treating process as well as that for GO and Gr. B) Raman spectra of GO and heat-treated Pt/N-Gr. C) XPS survey spectra of Gr and Pt/N-Gr (after the heat-treating process). D and E illustrate the high resolution scans of corresponding Pt 4f and N 1s XPS spectra, respectively.

These confirm successful incorporation of N atoms and anchoring Pt nanoparticle into the N-Gr sheets. The N/C atom ratio and the percentage of Pt in the nanostructure are calculated to be 3.1% and 6.84%, respectively. The recorded high resolution scan of Pt 4f peak (Fig. 2D) reveals that this peak is a combination of three pairs of doublets. The most intense doublet (71.2 and 74.5 eV) is associated to metallic Pt, indicating that most of Pt ions are reduced to metallic Pt during the potential cycling in the cathodic direction and heat-treating process. The second set of doublets at BE of 72.5 and 75.8 eV can be attributed to Pt(II). The last doublet with broader bands and lower intensities presented at 75.2 and 78.4 eV can be attributed to Pt(IV) species [17,43]. These results clearly indicate that the Pt nanoparticles successfully are integrated with N-Gr supporting sheets. On the other hand, the recorded high resolution scan of N 1s peak of the Pt/N-Gr (Fig. 2E) reveals that the incorporated N atoms into the Gr structure are mainly in the form of pyridine-like N (~398.4 eV) coexist with small amount of pyrolytic type (~399.6 eV) and larger amount of quaternary graphitic type N atoms (~401.0 eV) [17,28,29,44]. As mentioned above, the graphitic quaternary nitrogen, plays a significant role in the high electrocatalytic activity for ORR [13,27–29], with higher CO and methanol poisoning resistance.

The prepared composite was also characterized by taking FE-SEM and TEM images. Fig. 3 display FE-SEM and TEM images of both chemically synthesized Gr and electrochemically synthesized Pt/N-Gr based on the present method. In contrast to the pristine Gr sheets (Fig. 3A and C), the Gr sheets in the Pt/N-Gr sample are evenly decorated by Pt nanoparticles (Fig. 3B).

The TEM image of Pt/N-Gr sample (Fig. 3D) confirms a uniform distribution of Pt nanoparticles in the size of 2–20 nm on the N-Gr sheets. The results reconfirm that Pt nanoparticles are successfully incorporated with nitrogen doped Gr nanosheets through the proposed simple one-step electrochemical process. Corresponding EDX elemental and map analysis further confirm the results obtained by XPS and TEM (Figure S4).

3.2. Electrocatalytic activity of Pt/N-Gr/GC electrode toward ORR

The electrocatalytic performance of the synthesized Pt/N-Gr toward ORR was investigated by recording cyclic voltammograms of GC electrode modified with Pt/N-Gr. As illustrated in Fig. 4A, a well-defined cathodic peak at −0.18 V is clearly observed under O_2-atmosphere in 0.1 M KOH. The onset potential for O_2 reduction on the Pt/N-Gr modified GC electrode is ~0.05 V which about 0.1 V and 0.25 V more positive compared to the commercial Pt/C modified GC electrode and chemically synthesized Gr modified electrodes, respectively. On the other hand, the comparisons of ORR limiting current densities indicate that the electrocatalytic activity of Pt/N-Gr is almost 1.7 and 5.5 times rather than Pt/C and Gr, respectively. Furthermore, the long-term activities of Pt/N-Gr/GC electrode was also studied by recording sequence potential cycling, as shown after 400 continuous cycles a small decrease (~%3) in the current density was observed (Fig. 4A). The activity of electrode was further studied in H_2SO_4 and phosphate buffer solution (pH 7). As illustrated in Figure S5 the modified electrode also shows high catalytic activity in both natural and acidic solutions.

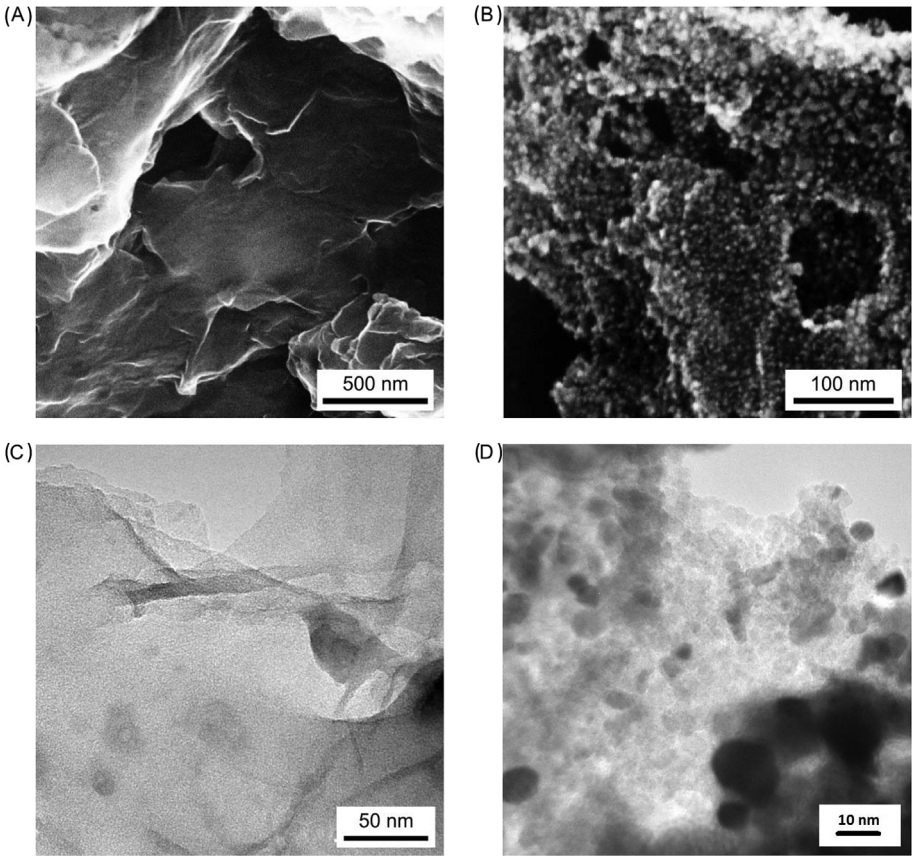

Fig. 3. FE-SEM images (with magnification of 42,000) of Gr (A) and Pt/N-Gr (with magnification of 190,000) synthesized by the proposed method (B). TEM images of Gr (C) and synthesized Pt/N-Gr (D).

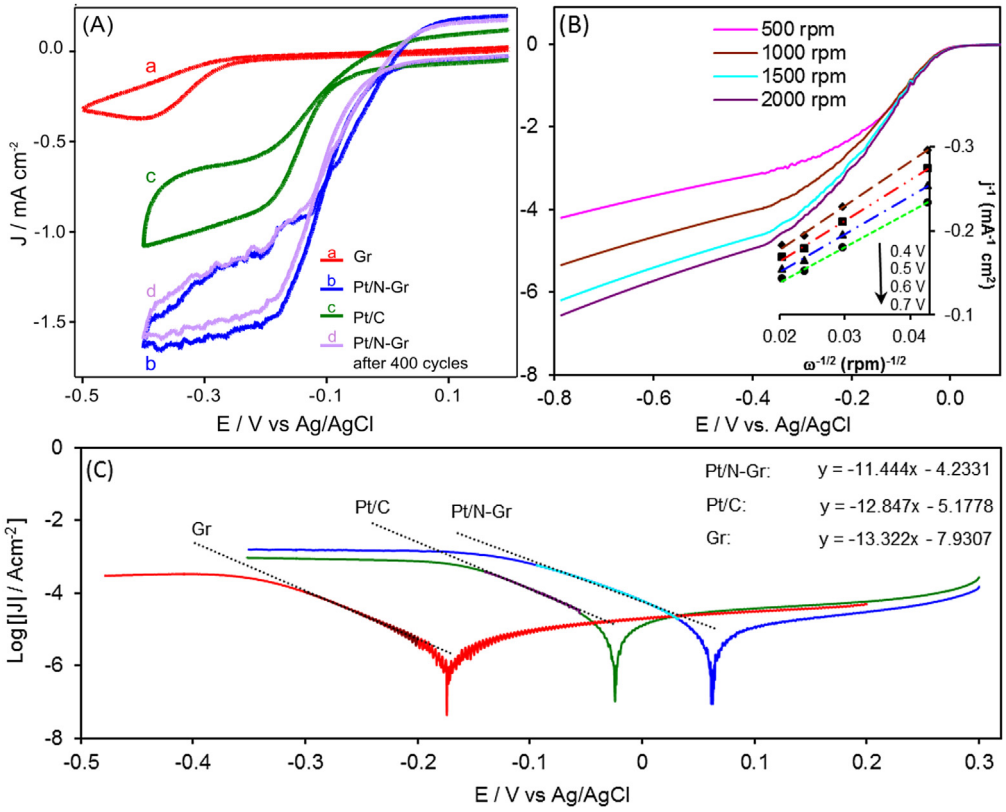

Fig. 4. A) CVs of ORR under O_2 saturated on the modified electrodes with Gr (a), Pt/N-Gr (b), Pt/C (c) and Pt/N-Gr after 400 successive cycles (d). B) Current density vs. potential for RDE of Pt/N-Gr in O_2-saturated for different speeds. The inset shows the Koutecky–Levich plots derived from the RDE measurements. C) Tafel plot based on the recorded CVs data for three types of electrodes. (Scan rate: 0.02 V s^{-1} in 0.1 M KOH solution).

To determine the number of transferred electron per O_2 molecule in the ORR process, linear sweep voltammetry (LSV) in 0.1 M KOH solution containing saturated O_2 was performed using rotating disc electrode (RDE) at various rotation rates. As seen in Fig. 4B, the current density increases with increasing rotation rates due to the enhancement in the mass transfer of O_2 [45]. By plotting the inverse of current density against the inverse square root of rotation rate (inset of Fig. 4B) and using the Koutecky–Levich equation [28,29] (see Supporting information), the number of transferred electron during the ORR on the Pt/N-Gr electrode is estimated 4 electron per one O_2 molecule. This result is in a good agreement to carbon materials supported Pt nanoparticles. So, the prepared Pt/N-Gr significantly improves the kinetics of O_2 reduction and facilitates the electron transfer rate.

To evaluate the kinetic parameters related to electrocatalytic property of Pt/N-Gr, Pt/C and Gr for the ORR including transfer coefficient (α) and rate of electron transfer at the electrode (k_{et}) the Tofel plots were drawn based on the recorded CVs at the cathodic direction (Fig. 4C). By the analysis the slopes and intercepts of linear curves which obtained from log $|J|$ vs. potential at the kinetic-control region, the kinetic parameters were calculated using the following equations (3) and (4) and the results presented in Table 1 [46]:

$$J_0 = nFk_{et}C \tag{3}$$

$$\text{slop} = \frac{-\alpha nF}{2.3RT} \tag{4}$$

where, J_o is the exchange current density equal to Tafel intercept and $C*$ is the bulk concentration of O_2 in 0.1 M KOH solution (1.25×10^{-6} mol cm^{-3}). In addition, n, F (96485 Coulombs), R (VC K^{-1} mol^{-1}) and T (298 Kelvin) are the number of electron transferred, Faraday constant, gas constant and ambient temperature, respectively. Taking into account the 4-electron reduction of O_2 on the all three electrodes, from the Tafel intercept and using equation (3) the amounts of k_{et} can be calculated. Moreover, the α values can be computed from the Tafel slope using equation (4) and as shown in Table 1 no significant difference between α values is observed. The comparison of the exchange current density and electron transfer rate constant for O_2 reduction at Pt/N-Gr reveals that these parameters dramatically increases by several orders of magnitude while, the amount of Pt at N-Gr (6.84%) is less than the amount of Pt on commercial Pt/C. These results signifying the fact that the Pt nanoparticles are incorporated with N-Gr structure and therefore, electron transfer kinetic for O_2 reduction are accelerated by this nanostructure.

Table 1
Comparison of electrochemical and kinetic parameters related to direct O_2 reduction by three types of electrodes.

Electrode	Onset potential/V vs Ag/AgCl	Tafel slope/ decadeV^{-1}	J_0/A cm^{-2}	α	k_{et}/cm s^{-1}
Gr	−0.20	13.32	1.2×10^{-8}	0.19	2.5×10^{-8}
Pt/C	−0.05	12.84	6.8×10^{-6}	0.19	1.4×10^{-5}
Pt/N-Gr	0.05	11.44	5.9×10^{-5}	0.17	1.2×10^{-4}

The alcohol oxidation intermediates poison the surfaces which diminish the catalytic activity of Pt and Pt/C electrodes is a major setback in both methanol-oxygen and ethanol-oxygen fuel cells. Fig. 5 represent the CVs of Pt/N-Gr (5A) and Pt/C (5B) modified electrodes in the O_2-saturated condition, 0.1 M methanol and

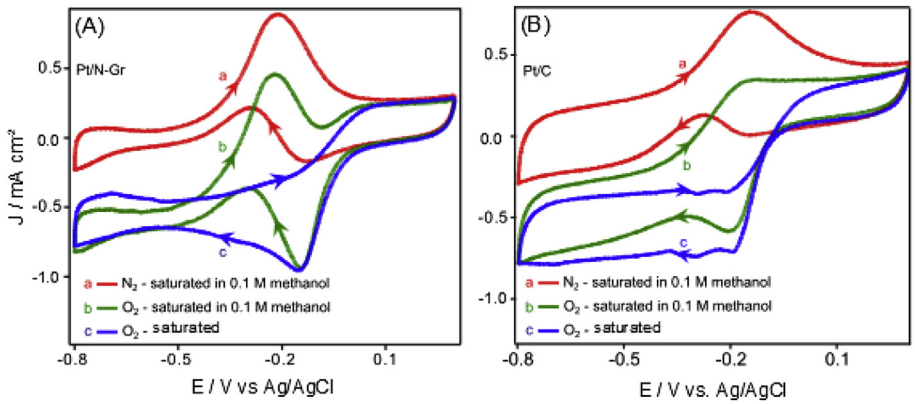

Fig. 5. A) CVs of N_2-saturated in the presence of 0.1 M methanol (a), O_2-saturated in presence of 0.1 M methanol (b) and O_2-saturated (c) on Pt/N-Gr modified electrode. B) CVs of N_2-saturated in presence of 0.1 M methanol (a), O_2-saturated in presence of 0.1 M methanol (b) and O_2-saturated (c) on Pt/C modified electrode (Scan rate: 0.02 V s^{-1} in 0.1 M KOH solution).

mixture of them. Unlike the Pt/C that the current density for the methanol–oxygen mixture is substantially decreased, for the case of Pt/N-Gr the differences in the current densities are not significant. Similar results were also obtained when electrodes examined in the mixture of O_2 and ethanol (Figure S6). These results clearly indicate high resistance of the Pt/N-Gr modified electrode against deactivation by alcohols oxidation intermediates.

3.3. Electrocatalytic activity of Pt/N-Gr/GC modified electrode for fuel oxidation

To explore the potential application of Pt/N-Gr as an anodic material for fuel cells, the electrooxidation of typical fuels such as ethanol and methanol was studied by recording the cyclic voltammograms of Pt/N-Gr modified electrode in alkaline solution containing proposed fuels. Fig. 6A shows the CVs for

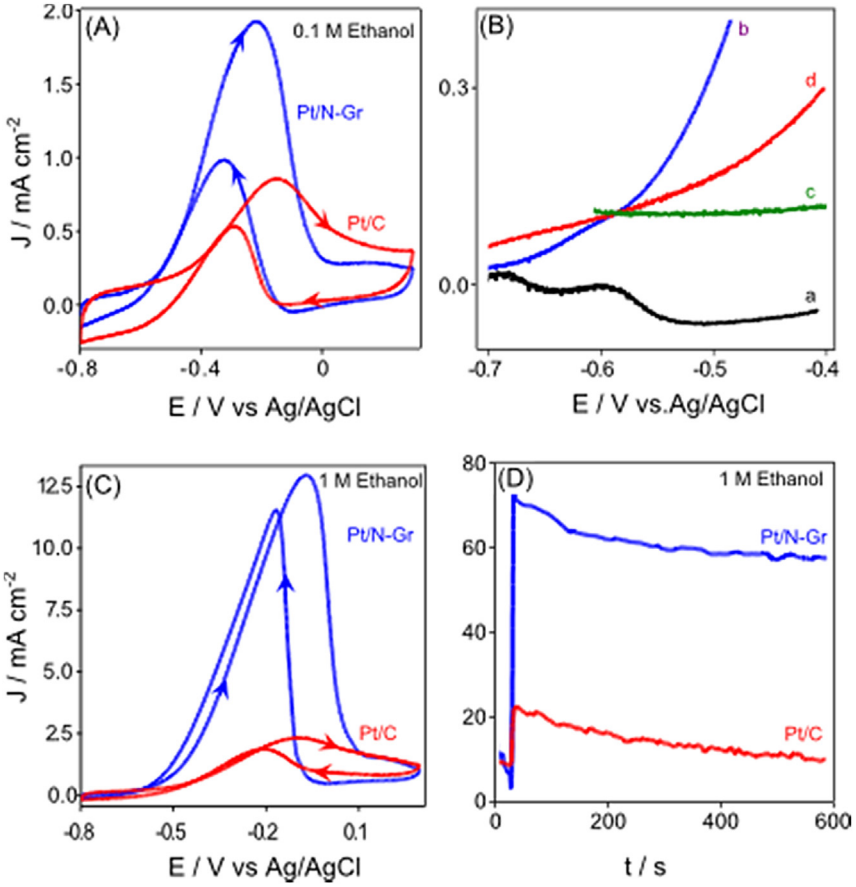

Fig. 6. A) CVs of 0.1 M ethanol oxidation on Pt/N-Gr (blue line) and Pt/C (red line). B) Enlarged section of onset peak potentials for ethanol oxidation for two types of catalyst (a and c represent the background current for Pt/N-Gr and Pt/C, respectively. b and d represent the catalytic current obtained by Pt/N-Gr and Pt/C, respectively). C) CVs of 1 M ethanol oxidation on Pt/N-Gr (blue line) and Pt/C (red line). D) Hydrodynamic chronoampreroetric response (500 rpm) of 1 M ethanol oxidation at −0.1 V on Pt/N-Gr and Pt/C in the 0.1 M KOH solution. (For interpretation of the references to color in this figure legend, the reader is referred to the web version of this article.)

electrooxidation of 0.1 M ethanol on Pt/N-Gr and Pt/C electrodes in 0.1 M KOH. For both electrodes, two typical oxidation peaks are observed in both forward and backward CV scanning (scan rate 0.02 V s^{-1}) due to the oxidations of ethanol and their intermediates, respectively [47]. The onset potential of ethanol electrooxidation for Pt/N-Gr is ~ −0.67 V that is 0.14 V more negative than that for Pt/C (Fig. 6B). Moreover, the height of the forward anodic peak for Pt/N-Gr is ~1.91 mA cm^{-2}, shows two folds enhancement rather than Pt/C (0.85 mA cm^{-2}). The significant improvement of the current density and decreasing of the overpotential oxidation can be attributed to the outstanding properties of N-Gr substrate [17,30–33,36–38] and accessible Pt nanoparticles which uniformly anchored into the N-Gr sheets. Fig. 6C compares the recorded CVs of electrooxidation of 1 M ethanol on Pt/N-Gr and Pt/C where, the current density on the Pt/N-Gr is recorded as 12.81 mA cm^{-2}, almost 6.88 times higher than that for Pt/C (1.86 mA cm^{-2}). So, with comparison of current densities for electrooxidation of 0.1 and 1 M ethanol, there is a proportional relationship between current density and ethanol concentration for the case of Pt/N-Gr compared to Pt/C. Fig. 6D shows the recorded hydrodynamic chronoamperograms of Pt/N-Gr and Pt/C modified GC electrodes in 1 M ethanol at −0.1 V during a period of 600 s. The current density from ethanol oxidation on Pt/N-Gr is ~6 times higher than that for Pt/C, and only 12% decay observed over 600 s compared to 30% decay for the case of Pt/C. These results signify higher activity and poisoning tolerance of Pt/N-Gr compared to Pt/C.

The electrocatalytic ability of the Pt/N-Gr modified electrode toward oxidation of methanol was also investigated. As shown in Figure S7, Pt/N-Gr exhibits favorable electrocatalytic activity toward methanol oxidation, although higher activity toward ethanol oxidation can be observed in comparison to methanol oxidation. These results clearly indicate the high activity of the composite which was derived via our proposed method toward direct alcohol oxidation.

The ability of Pt/N-Gr catalyst to perform as an anode material is further investigated through examination of its catalytic behavior toward oxidation of two typical fuels, hydrazine and formic acid. Fig. 7A exhibits the typical recorded CVs of electrooxidation of hydrazine in 0.1 M KOH on Pt/N-Gr and commercial Pt/C catalyst. As can be seen, there are two broad anodic CV peaks in the forward scans with the onset potential of −0.82 V for Pt/N-Gr and −0.79 V for Pt/C. The anodic peak potential for Pt/N-Gr is positioned at about −0.68 V, which is 0.2 V more negative than that for Pt/C. On the other hand, the electrocatalytic current density for hydrazine oxidation on Pt/N-Gr modified GC electrode is 2.55 times higher than observed value at Pt/C modified GC electrode. Fig. 7B represents the CVs of electrooxidation of formic acid on Pt/N-Gr and Pt/C in 0.5 M H_2SO_4 solution. As shown, two distinct oxidation peaks can be seen in the forward and backward CV scanning, arising from the oxidation of formic acid and their intermediates. There are clear differences between the catalytic activity of Pt/N-Gr and Pt/C toward oxidation of formic acid. Also the limiting current density for Pt/N-Gr is much higher than that for Pt/C ~1.61 times in the forward scan. Furthermore, as can be seen the onset potential for formic acid oxidation at Pt/N-Gr modified electrode is started at −0.03 V, while for the case of Pt/C modified electrode it is about 0.3 V. The higher current density in the backward scan is generally regarded as a disadvantage for the catalytic activity of Pt/N-Gr toward formic acid oxidation; indicate an inefficiency of the catalyst in oxidizing the reaction intermediates of formic acid during the forward scan.

The increasing of electrocatalytic limiting current in the forward scan and decreasing of overvoltage indicate the outstanding electroctalytic activity of Pt/N-Gr toward hydrazine and formic acid oxidation compared to Pt/C. So, the Pt/N-Gr nanostructure has high catalytic activity toward oxidation of alcohols, hydrazine and formic acid as typical anodic fuels. These interesting results may be as consequences of preferable anchoring Pt catalyst on N-Gr substrate where, the Pt/N-Gr takes the advantageous of both Pt nanoparticles and N-doped graphene as well. The recorded hydrodynamic chronoamperograms of Pt/N-Gr and Pt/C modified GC electrodes in 1 M hydrazine at −0.7 V during a period of 700 s are shown in Figure S8. As illustrated the current density for hydrazine oxidation on Pt/N-Gr is ~3.5 times higher than that for Pt/C, and only 15% decay is observed over 700 s compared to 45% decay for the case of Pt/C. These results signify higher activity and poisoning tolerance of Pt/N-Gr compared to Pt/C.

4. Conclusion

For the first time, we developed a direct one-step electrochemical approach for preparation of nitrogen doped Gr nanosheets that support platinum nanoparticle. The electrosynthesized composite was characterized using spectroscopic and imaging techniques. In comparison to commercial Pt/C the prepared Pt/N-Gr

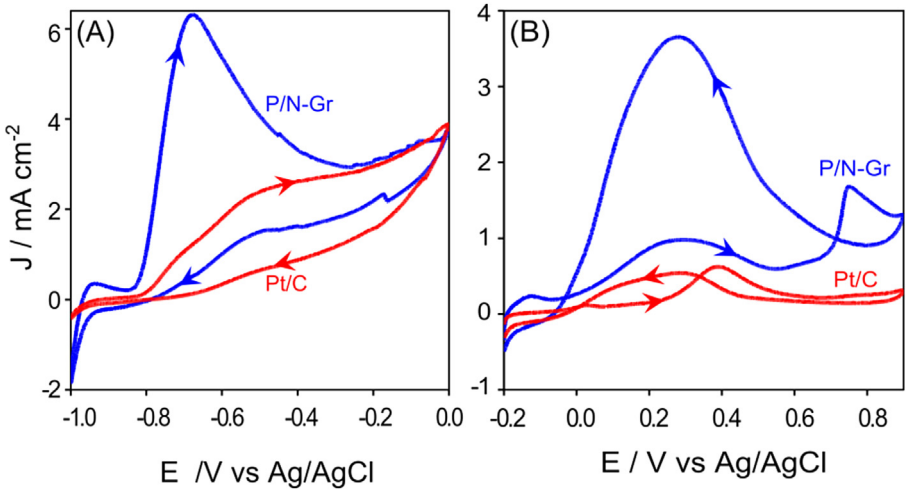

Fig. 7. A) CVs of electrocatalytic oxidation of 0.20 M of hydrazine hydroxide in 0.1 M KOH on Pt/N-Gr (blue line) and Pt/C (red line). B) CVs of 0.44 M of formic acid in the N_2-saturated 0.5 M H_2SO_4 solution on Pt/N-Gr (blue line) and Pt/C (red line). (The scan rate of all CVs is 0.02 V s^{-1}). (For interpretation of the references to color in this figure legend, the reader is referred to the web version of this article.)

exhibited remarkable electrocatalytic activity for both oxygen reduction reaction and oxidation of ethanol, methanol, hydrazine, and formic acid as typical anodic fuels. Furthermore, decoration of N-Gr sheets nanoparticle by Pt nanoparticles not only enhanced its electrocatalytic activity, but also decreased the poisoning effect of fuels and their oxidation products/intermediates, which is a serious limitation for the commercial Pt/C catalysts. Hence, the results signify the ability of Pt/N-Gr that can be used as an anodic and cathodic catalyst in fuel cells. The proposed method is simple, low cost and scalable for production of Pt/N-Gr. This method can also be easily extendable to large-scale synthesis of other metal/graphene nanostructures in the future.

Acknowledgments

This research was supported by the Iranian Nanotechnology Initiative and the Research Office of the University of Kurdistan. The authors acknowledged Dr Rezgar Ahmadi for his corporation in analysis of XPS data.

Appendix A. Supplementary data

Supplementary data related to this article can be found at http://dx.doi.org/10.1016/j.jpowsour.2014.11.117.

References

[1] M. Armand, J.M. Tarascon, Nature 451 (2008) 652–657.
[2] E.M. Erickson, M.S. Thorum, R. Vasic, N.S. Marinkovic, A.I. Frenkel, A.A. Gewirth, R.G. Nuzzo, J. Am. Chem. Soc. 134 (2012) 197–200.
[3] S. Wang, E. Iyyamperumal, A. Roy, Y. Xue, D. Yu, L. Dai, Angew. Chem. Int. Ed. 50 (2011) 11756–11760 (and reference therein).
[4] H. Song, X. Qiu, F. Li, Appl. Catal. A. Gen. 364 (2009) 1–7.
[5] K. Asazawa, K. Yamada, H. Tanaka, A. Oka, M. Taniguchi, T. Kobayashi, Angew. Chem. Int. Ed. 46 (2007) 8024–8027.
[6] A. Serov, C. Kwak, Appl. Catal. B: Environ. 98 (2010) 1–9.
[7] E. Antolini, Energy Environ. Sci. 2 (2009) 915–931.
[8] R. Lan, S. Tao, Electrochem. Solid-State Lett. 13 (2010) B83–B86.
[9] M. Winter, R.J. Brodd, Chem. Rev. 104 (2004) 4245–4269.
[10] X. Yu, P.G. Pickup, J. Power. Sources 187 (2009) 493–499.
[11] H. Liu, C. Song, L. Zhang, J. Zhang, H. Wang, D.P. Wilkinson, J. Power Sources 155 (2006) 95–110.
[12] W. Li, Q. Xin, Y. Yan, Int. J. Hydrogen Energy 35 (2010) 2530–2538.
[13] Y. Zheng, Y. Jiao, M. Jaroniec, Y. Jin, S.Z. Qiao, Small 8 (2012) 3550–3566.
[14] A.O. Neto, M. Linardi, D.M. dos Anjos, G. Tremiliosi, E.V. Spinace, J. Appl. Lectrochem 39 (2009) 1153–1156.
[15] C. Pan, Y. Li, Y. Ma, X. Zhao, Q. Zhang, J. Power Sources 196 (2011) 6228–6231.
[16] S. Du, Y. Lu, S.K. Malladi, Q. Xu, R. Steinberger-Wilckens, J. Mater. Chem. A 2 (2014) 692–698.
[17] B. Xiong, Y. Zhou, Y. Zhao, J. Wang, X. Chen, R. O'Hayre, Z. Shao, Carbon 52 (2013) 181–192 (and reference therein).
[18] A.K. Geim, K.S. Novoselov, Nat. Mater. 6 (2007) 183–191.
[19] H.J. Choi, S.M. Jung, J.M. Seo, D.W. Chang, L. Dai, J.B. Baek, Nano Energy 1 (2012) 534–551.
[20] S. Sun, G. Zhang, N. Gauquelin, N. Chen, J. Zhou, S. Yang, W. Chen, X. Meng, D. Geng, M.N. Banis, R. Li, S. Ye, S. Knights, G.A. Botton, T.K. Sham, X. Sun, Sci. Rep. 3 (2013) 1–9.
[21] S. Sattayasamitsathit, Y. Gu, K. Kaufmann, W. Jia, X. Xiao, M. Rodriguez, S. Minteer, J. Cha, D.B. Burckel, C. Wang, R. Polsky, J. Wang, J. Mater. Chem. A 1 (2013) 1639–1645 (and reference therein).
[22] D.W. Boukhvalov, M.I. Katsnelson, Nano Lett. 8 (2008) 4373–4379.
[23] L.S. Panchakarla, K.S. Subrahmanyam, S.K. Saha, A. Govindaraj, H.R. Krishnamurthy, U.V. Waghmare, C.N.R. Rao, Adv. Mater. 21 (2009) 4726–4730.
[24] X.L. Li, H.L. Wang, J.T. Robinson, H. Sanchez, G. Diankov, H.J. Dai, J. Am. Chem. Soc. 131 (2009) 15939–15944.
[25] T. Maiyalagan, X. Dong, P. Chen, X. Wang, J. Mater. Chem. 22 (2012) 5286–5290.
[26] P. Nath, S. Chowdhury, D. Sanyal, D. Jana, Carbon 73 (2014) 275–282.
[27] R. Liu, D. Wu, X. Feng, K. Mullen, Angew. Chem. Int. Ed. 49 (2010) 2565.
[28] L. Qu, Y. Liu, J.B. Baek, L. Dai, ACS Nano 4 (2010) 1321–1326.
[29] Y. Li, Y. Zhao, H. Cheng, Y. Hu, G. Shi, L. Dai, L. Qu, J. Am. Chem. Soc. 134 (2012) 15–18.
[30] D. Yu, L. Wei, W. Jiang, H. Wang, B. Sun, Q. Zhang, K. Goh, R. Si, Y. Chen, Nanoscale 5 (2013) 3457–3464.
[31] X. Xu, Y. Zhou, T. Yuan, Y. Li, Electrochim. Acta 112 (2013) 587–595.
[32] Y. Zhao, Y. Zhou, R. O'Hayre, Z. Shao, J. Phys. Chem. Sol. 74 (2013) 1608–1614.
[33] X.R. Wang, X.L. Li, L. Zhang, Y. Yoon, P.K. Weber, H.L. Wang, J. Guo, H.J. Dai, Science 324 (2009) 768–771.
[34] P. Kannan, T. Maiyalagan, N.G. Sahoo, M. Opallo, J. Mater. Chem. B 1 (2013) 4655–4666.
[35] S. Wang, L. Zhang, Z. Xia, A. Roy, D.W. Chang, J.B. Baek, L. Dai, Angew. Chem. Int. Ed. 51 (2012) 1–5.
[36] K. Tiido, N. Alexeyeva, M. Couillard, C. Bock, B.R. MacDougall, K. Tammeveski, Electrochim. Acta 107 (2013) 509–517.
[37] M.H. Seo, S.M. Choi, H.J. Kim, W.B. Kim, Electrochem. Commun. 13 (2011) 182–185.
[38] D. Geng, Y. Hu, Y. Li, R. Li, X. Sun, Electrochem. Commun. 22 (2012) 65–68.
[39] A. Navaee, A. Salimi, H. Teymourian, Biosens. Bioelectron. 31 (2012) 205–211.
[40] D. Aurbach, I. Weissman, Nonaqueous Electrochemistry, Marcel Dekker, Inc, 270 Madison Avenue, New York, NY 10016, 1999.
[41] R. Pazout, J. Houskova, M. Dusek, J. Maixner, J. Cibulkova, P. Kacer, Acta Cryst. C. 66 (2010) 273–275.
[42] K. Nakamoto, Infrared and Raman Spectra of Inorganic and Coordination Compounds, sixth ed., John Wiley & Sons, Inc, 2009.
[43] M.Y. Yen, C.C. Teng, M.C. Hsiao, P.I. Liu, W.P. Chuang, C.C.M. Ma, C.K. Hsieh, M.C. Tsai, C.H. Tsai, J. Mater. Chem. 21 (2011) 12880–12888.
[44] Y. Zhong, M. Jaidann, Y. Zhang, G. Zhang, H. Liu, M.I. Ionescu, R. Li, X. Sun, H.A. Rachid, L.S. Lussier, J. Phys. Chem. Sol. 71 (2010) 134–139.
[45] C.B. Tobias, M. Eisenberg, C.R. Wilke, J. Electrochem. Soc. 99 (1952) 359–365.
[46] A.J. Bard, L.R. Faulkner, Electrochemical Methods. Fundamentals and Applications, Second ed., Wiley, 2001.
[47] A.S. Aarnio, Y. Kwon, E. Ahlberg, K. Kontturi, T. Kallio, M.T.M. Koper, Electrochem. Commun. 13 (2011) 466–469.